Injection Locking and Phase Control of Spin Transfer Nano-oscillators

W. H. Rippard, M. R. Pufall, S. Kaka, T. J. Silva, and S. E. Russek
National Institute of Standards and Technology, Boulder, Colorado 80305, USA

J. A. Katine
Hitachi Global Storage Technologies, San Jose, California 95120, USA
(Received 17 March 2005; published 5 August 2005)

We have directly measured phase locking of spin transfer oscillators to an injected ac current. The oscillators lock to signals up to several hundred megahertz away from their natural oscillation frequencies, depending on the relative strength of the input. As the dc current varies over the locking range, time-domain measurements show that the phase of the spin transfer oscillations varies over a range of approximately $\pm 90°$ relative to the input. This is in good agreement with general theoretical analysis of injection locking of nonlinear oscillators.

DOI: 10.1103/PhysRevLett.95.067203 PACS numbers: 85.75.−d, 05.45.Xt, 75.75.+a

Synchronization of weakly coupled oscillators, generally referred to as injection locking or frequency entrainment, has numerous examples in nature and generally occurs in oscillator systems having at least weak nonlinear interactions. Examples range from biological systems, such as the synchronized flashing of fireflies and singing of certain crickets, to those in the physical sciences, such as Josephson junction arrays and the synchronization of the Moon's rotation with respect to its orbit around the Earth. This feature is exploited in many modern technologies such as wireless communications, the American power grid, various power combining architectures, and phased array antennae networks [1]. One of the simplest methods of synchronizing electronic based oscillators is through the application of an ac signal close to the oscillator's natural frequency, inducing the device to oscillate sympathetically at the drive frequency. One of the first theoretical descriptions of such behavior was given by Adler [2]. While his analysis was specifically for a vacuum tube and resistor-inductor-capacitor (RLC) circuit, this simple analysis has been found to describe numerous other nonlinear oscillators as well.

The oscillators discussed in this Letter are based on the spin transfer effect in which a dc current transfers spin angular momentum from a "fixed" ferromagnetic film to the magnetic moment of a second "free" ferromagnetic film, inducing coherent precession of the magnetization of the second layer [3–7]. The frequency of precession f for these oscillators can be tuned from a few GHz to >40 GHz by changing the magnetic field strength and dc current applied to the devices, effectively resulting in a voltage (current) controlled oscillator [7]. In this Letter we demonstrate that the same basic analysis used for discrete resonator circuits and classical nonlinear oscillators can also be applied to these more recent nanometer-scale spin-electronic devices.

The sample consists of a nominally 50 nm diameter electrical contact to the top of a 10 μm × 20 μm spin-valve mesa composed of SiO_2/Ta(5 nm)/Cu(50 nm)/$Co_{90}Fe_{10}$(20 nm)/Cu(4 nm)/$Ni_{80}Fe_{20}$(5 nm)/Cu(1 nm)/Au(1 nm). The device has a dc resistance of 15 Ω and a $\Delta R_{max} = 180$ mΩ [8]. In this geometry the CoFe is considered the fixed layer and the NiFe is considered the free layer, due to differences in their thicknesses and saturation magnetizations [3]. The devices are dc current biased, producing driven precession of the free layer [see inset Fig. 1(a)]. This precession generates a microwave voltage due to the giant magnetoresistance effect. Micromagnetic simulations indicate that the magnetization directly under the contact precesses uniformly and radiates spin waves with a wavelength of roughly 100 nm and a spatial extent of several hundred nanometers, in agreement with previous measurements [7].

All data presented here are from a single device measured at room temperature with an external field $\mu_0 H = 560$ mT applied at angle 75° to the film plane. Simulations

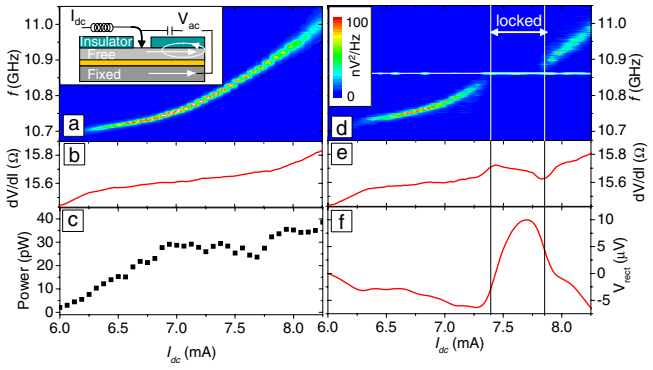

FIG. 1 (color online). (a) Plot of f vs I_{dc} with amplitude shown in a linear color scale from 0 (black) to 100 nV^2/Hz (light) with (b) corresponding dV/dI curve without ac drive. Inset: Device and measurement schematic. (c) Device output power vs I_{dc} without ac drive signal in the same color scale. (d),(e) Same as in (a),(b) but with an ac drive at 10.86 GHz, 410 μA^{rms}. (f) Plot of V_{rect} vs I_{dc}. Vertical lines indicate the region of locking.

indicate that this geometry will induce precession of the free-layer magnetization in a quasicircular orbit around its equilibrium direction with the precession angle varying with I_{dc}, as discussed in Refs. [4,7]. The same behaviors discussed here have been measured in other devices and geometries, although the details of the behaviors vary, as discussed below. The devices are contacted with microwave probes, and a bias tee is used to separate the high-frequency device response from the dc current bias I_{dc}. A high-frequency current can be added to I_{dc} through the ac leg of the bias tee. The rf output from the device is measured with either a spectrum analyzer or a sampling oscilloscope.

The device output as a function of I_{dc} is shown in Fig. 1(a) along with the corresponding differential resistance curve, Fig. 1(b). The small feature in the dV/dI curve at 6.25 mA corresponds to the onset of oscillations in the f vs I_{dc} response. The power associated with the oscillations is shown in Fig. 1(c). In Figs. 1(d) and 1(e) we show the analogous data when an ac current $I_{ac}^{(rms)} = 410\ \mu$A at 10.86 GHz ($f_{drive}$) is added to I_{dc}. In our measurement, part of this ac signal is parasitically input to the spectrum analyzer used to acquire the data, and produces a background signal at 10.86 GHz in Fig. 1(d). We have found that in this configuration the spectrum analyzer lacks sufficient dynamic range to repeatedly subtract off this parasitic background, and so we are unable to directly measure the device output at this particular frequency using this method. At low currents the oscillation frequency is only slightly pulled towards the drive frequency f_{drive}. As I_{dc} is increased, the deviation between the driven and nondriven frequencies increases as the spin transfer oscillations are pulled closer to the drive frequency. At $I_{dc} = 7.4$ mA the device locks to the drive frequency, as we show explicitly below, and remains so until $I_{dc} = 7.8$ mA. Single domain simulations indicate that throughout the locking range the magnetization follows the same trajectory as when oscillating at that same frequency in response to only a dc current. At larger currents the device oscillation frequency is distinct from the drive frequency but is again pulled towards f_{drive}. Over the locking range of the oscillator a dc rectified voltage V_{rect} is measured, Fig. 1(f). As discussed in Ref. [6], this gives indirect evidence of injection locking of the oscillator to the input signal.

When locked, the oscillator is expected to take on the noise characteristics of the injected signal [9]. A frequency stability of $f/\Delta f > 10^9$ is expected in the present case as determined by the microwave source, allowing measurement of the signal using stroboscopic sampling techniques. Direct measurement of the oscillator synchronization is done in the time domain using a sampling oscilloscope instead of the spectrum analyzer. The oscilloscope is triggered from a 10 MHz signal that is phase referenced to the microwave generator. The signal measured by the oscilloscope is again composed of both a background signal from the microwave generator and the output from the spin transfer device. To determine the device output, the background signal is first measured with no current running through the device. A second measurement is then taken with I_{dc} through the device and the background signal is subtracted, leaving the output from the device. Typically about 1000 averages are acquired for each time trace. In principle, this measurement is equivalent to the one using a spectrum analyzer. However, the dynamic range of the sampling oscilloscope is larger ($1{:}2^{15}$) than that of the spectrum analyzer, permitting repeatable subtraction of the background signal. Such a stroboscopic measurement technique gives a null result unless the output from the device is phase synchronous with the injected microwave signal (i.e., the trigger signal) throughout the entire measurement interval of about 5 min.

As indicated in Fig. 1(d), the oscillator is locked to the injected signal for $I_{dc} = 7.6$ mA. A time trace corresponding to this locked state is shown in Fig. 2(a) along with a sinusoidal fit. The fact that we are able to measure the signal in the time domain explicitly shows that the oscillator is phase locked to the injected signal. A fit to the data yields an oscillation frequency of 10.86 GHz and a peak voltage of 44 μV. A spectral measurement of the device output without an ac bias for $I_{dc} = 7.6$ mA is shown in Fig. 2(b). The spectral signal is equivalent to a peak voltage of 51 μV, in good agreement with the time-domain signal. Spectral measurements indicate that no significant power is generated at other frequencies (0–40 GHz). The deviation of the signal from a sinusoid is likely the result of imperfect synchronization between the trigger and the injected signal, as similar deviations from a sinusoid are obtained when directly measuring the microwave generator output.

The effect of varying the dc current through the locking range is shown in Fig. 3(a). The device is locked to an ac current of $I_{ac}^{rms} = 410\ \mu$A at 10.86 GHz, and the time-domain signal is measured as I_{dc} is varied from 7.2 to 7.8 mA. As seen in the figure, the phase of the spin transfer oscillator varies relative to that of the injected signal, allowing electronic phase control of the devices. Over the locking range the phase of the device varies through roughly $\pm 90°$, as shown in Fig. 3(b). No time-domain

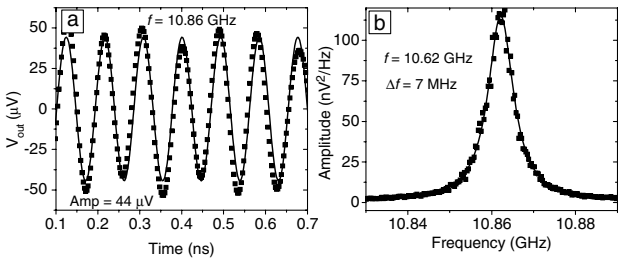

FIG. 2. (a) Time-domain measurement of device output at $I_{dc} = 7.6$ mA along with a sinusoidal fit (line). (b) Spectral measurement of the device output with the same bias I_{dc} along with a fit to a Lorentzian function.

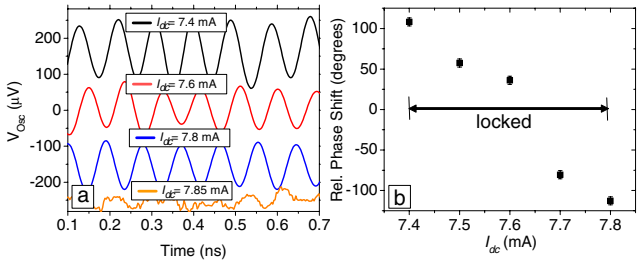

FIG. 3 (color online). (a) Time-domain measurements of the device output as a function of dc current bias. The data are offset for clarity. (b) Relative phase shift between the device output and the external drive signal. An overall phase of 100° has been subtracted from the data.

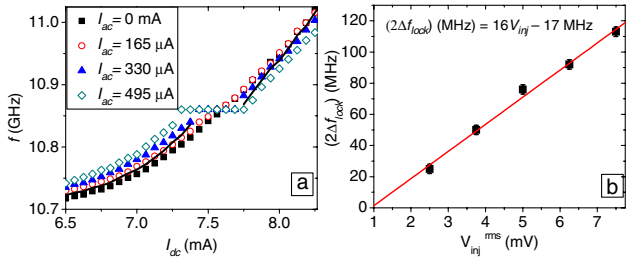

FIG. 4 (color online). (a) Plot showing the f vs I_{dc} relation for several different amplitudes of drive at 10.86 GHz. The solid line is the predicted oscillation frequency for the drive of 330 μA, as discussed in the text. (b) Plot showing the locking range as a function of ac drive amplitude (ac voltage across the device) along with a linear fit to the data.

signals are observed outside this range, indicating that the signal is no longer phase coherent with the injected signal, as shown by the $I_{dc} = 7.85$ mA data.

We compare our results to the model of Adler, which treats the oscillator as an active nonlinear circuit element coupled to an RLC circuit [2]. While simple, this analysis has been found to describe the locking characteristics of a range of oscillator circuits such as those based on diodes, transistors, and klystrons, to name a few [1,2,10]. The basic result of the analysis is

$$f_{\mathrm{drive}} - f_{\mathrm{o}} = \Delta f_{\mathrm{lock}} \sin(\phi); \qquad \Delta f_{\mathrm{lock}} = \frac{\Delta f}{2} \frac{V_{\mathrm{inj}}}{V_{\mathrm{osc}}}, \quad (1)$$

where Δf_{lock} defines the locking range of the device, Δf is the free-running oscillation linewidth, f_{o} is the free-running oscillation frequency, V_{inj} is the injected ac voltage across the device, V_{osc} is the oscillator voltage output, and ϕ is the phase difference between the oscillator and the injected signal. Equation (1) has a solution for $f_{\mathrm{drive}} = f_{\mathrm{o}} \pm \Delta f_{\mathrm{lock}}$, and over that range the phase of the oscillator relative to the injected signal varies from $-90° < \phi < 90°$, in agreement with the data in Fig. 3. Equation (1) is derived under the limit that the addition of the injected signal does not significantly alter the output amplitude of the oscillator. In our devices this criterion is met as long as the oscillator output (amplitude and linewidth) does not too strongly depend on the dc bias current over the locking range. This is often the case, as it is for the data presented here [see Fig. 1(c)]. In other cases deviations from the 180° phase shift and the simple linear dependence of the locking range on the injected signal strength are found, as expected when significant power variation is included in the model [11].

The dependence of the oscillation frequency on dc current for several different ac injection amplitudes is shown in Fig. 4(a). The oscillation frequency is determined by Lorentzian fits to the spectral measurements and I_{ac} is estimated using standard microwave circuit analysis and taking the rf device resistance as equivalent to its dc value with no complex components [12]. As was seen in Fig. 1, when the device is biased outside of the locking range, the spectral measurements indicate that the oscillation frequency is pulled towards the injected ac signal. The measured frequency is only slightly pulled from its nondriven value far from the locking region. However, when the device is just outside of the locking range, the effect of the frequency pulling is much more significant, with the measured frequency continuously approaching the injection frequency. This is not a frequency modulation effect. In modulation schemes the frequency of the mixed signal is independent of the amplitude of the modulation signal, at least for a linear f vs I relationship [13]. As seen in Fig. 4(a) this is not the case. Instead, the measurements are consistent with the oscillator quasilocking to the injected signal. As is discussed in Ref. [9], when the oscillator is close to but outside the locking range, the device undergoes periods of being locked to the injected signal, punctuated by periods when the oscillator undergoes rapid phase slips and oscillates at frequencies different from f_{drive}. The closer the oscillator is to the locking range, the longer the time between these periods of rapid phase change. The result is that the device does not oscillate at a single frequency but over a range of frequencies, which appears as the pulling effect shown in Fig. 4.

In Fig. 4(b), the full locking range $(2\Delta f_{\mathrm{lock}})$ is more explicitly shown as a function of the drive amplitude. The locking range is taken as the difference between the nondriven device oscillation frequencies at the minimum and maximum dc currents at which the device locks to the injected signal, and the device is taken to be locked to the injected signal when more than 90% of the oscillator signal is at the injection frequency. The locking range varies approximately linearly with drive amplitude with a slope of 16 MHz/mV. From Eq. (1), the full locking range is expected to be linear with a slope of $(\Delta f / V_{\mathrm{osc}})$ and intersect the origin. The slope predicted by Eq. (1) can only be estimated since the quantity depends explicitly upon the device output. While the cabling and other component insertion losses can be measured, the coupling coefficient between our low impedance devices and a 50 Ω microwave line must be calculated [12]. For the

$\Delta f = 7$ MHz device investigated here, we estimate that Eq. (1) predicts a slope of 42 MHz/mV. The remaining discrepancy is possibly accounted for by a difference between the dc device resistance used in our estimate and the actual device impedance at 10.86 GHz.

The quantitative difference between the slope predicted by Eq. (1) and the measured value is not constant but instead varies with the device studied and the measurement geometry. To date the values have always been within a factor of 5. For other devices in the same measurement geometry and a given injection amplitude, devices having larger linewidths and lower output powers lock over a wider range of frequencies, in accordance with Eq. (1). In general, the devices can be locked to signals up to several hundred MHz away from their natural oscillation frequency. The fit to the data indicates that a drive of finite amplitude, 1 ± 0.2 mV, is required to lock the device. This is in contrast to the predictions of Eq. (1). We have not yet determined the cause of the nonzero intercept, but it may reflect additional intrinsic losses in the nanocontact devices due to magnon radiation away from the device area [3].

Close to the locking range, spectral measurements of the oscillations are predicted to yield $f = f_{\mathrm{drive}} \pm [(f_{\mathrm{o}} - f_{\mathrm{drive}})^2 - \Delta f_{\mathrm{lock}}{}^2]^{0.5}$ [9]. The line in Fig. 4(a) shows this dependence for the data with $I_{\mathrm{ac}}{}^{\mathrm{rms}} = 330\ \mu$A. As seen in the figure, this qualitatively describes the data close to the locking region. However, as the device frequency gets farther away from the locking regime, the measured frequency pulling is significantly larger than the prediction. This discrepancy likely results from the amplitude effects that are not taken into account in our simple oscillator model [see Fig. 1(c)].

In summary, we have demonstrated that spin transfer oscillators can be injection locked to an ac current. Over the locking range, the phase of the device can be electronically tuned by approximately $\pm 90°$ in reference to the drive. The locking ranges are in qualitative agreement with the general theoretical analysis of nonlinear oscillators. These measurements indicate the potential for spin transfer based oscillators in practical microwave circuits that require synchronization of multiple oscillators (such as in timing circuits, signal tracking and reception, and signal demodulation) and phase control of multiple oscillators (such as directional beam steering, phased array detection, and localized coherent manipulation of quantum states).

This work was supported by the DARPA SpinS program and the NIST nanomagnetodynamics program. We acknowledge S. Wolf for motivating the work on phase control.

[1] S. Strogatz, *Sync* (Hyperion, New York, 2003); A. Pikovsky, M. Rosenblum, and J. Kurths, *Syncronization: A Universal Concept in Non-linear Sciences* (Cambridge University Press, Cambridge, 2001); J. J. Lynch, H.-C. Chang, and R. A. York, in *Active and Quasi-Optical Arrays for Solid-State Power Combining*, edited by R. York and Z. Popovic (John Wiley & Sons, New York, 1997), and references therein.

[2] R. Adler, Proc. IEEE **61**, 1380 (1973).

[3] J. C. Slonczewski, J. Magn. Magn. Mater. **159**, L1 (1996); **195**, L261 (1999); L. Berger, Phys. Rev. B **54**, 9353 (1996).

[4] M. D. Stiles and A. Zangwill, Phys. Rev. B **66**, 014407 (2002); K. J. Lee *et al.*, Nat. Mater. **3**, 877 (2004); S. M. Rezende, F. M. de Aguiar, and A. Azevedo, Phys. Rev. Lett. **94**, 037202 (2005); S. Zhang, P. M. Levy, and A. Fert, Phys. Rev. Lett. **88**, 236601 (2002); J. Z. Sun, Phys. Rev. B **62**, 570 (2000); S. E. Russek *et al.*, Phys. Rev. B **71**, 104425 (2005); B. Montigny and J. Miltat, J. Appl. Phys. (to be published); A. Slavin and P. Kabos, IEEE Trans. Magn. **41**, 1264 (2005); G. Bertotti *et al.*, Phys. Rev. Lett. **94**, 127206 (2005).

[5] I. N. Krivorotov *et al.*, Science **307**, 228 (2005); S. I. Kiselev *et al.*, Nature (London) **425**, 380 (2003); M. Tsoi *et al.*, Phys. Rev. Lett. **80**, 4281 (1998); M. Covington *et al.*, Phys. Rev. B **69**, 184406 (2004).

[6] M. Tsoi *et al.*, Nature (London) **406**, 46 (2000).

[7] W. H. Rippard *et al.*, Phys. Rev. Lett. **92**, 027201 (2004); W. H. Rippard *et al.*, Phys. Rev. B **70**, 100406 (2004).

[8] The NiFe and CoFe layers have coercivities and saturation magnetizations of 2 mT, 4 mT, 0.8 T, and 1.8 T, respectively.

[9] B. Razavi, IEEE J. Solid-State Circuits **39**, 1415 (2004).

[10] See, for example, R. A. York, IEEE Trans. Microwave Theory Tech. **41**, 1799 (1993), and references therein.

[11] K. Fukumoto, M. Nakajima, and J.-I. Ikenoue, IEEE Trans. Microwave Theory Tech. **83**, 954 (1983).

[12] C. T. A. Johnk, *Engineering Electromagnetic Fields and Waves* (John Wiley & Sons, New York, 1988), 2nd ed.

[13] M. R. Pufall *et al.*, Appl. Phys. Lett. **86**, 082506 (2005).